

See discussions, stats, and author profiles for this publication at: <https://www.researchgate.net/publication/232061740>

Nanoparticle Supported Magnetically-Recoverable Oxodiperoxo Molybdenum Complexes: Efficient Catalysts for Selective Epoxidation Reactions

DATASET · OCTOBER 2012

READS

131

6 AUTHORS, INCLUDING:



Julia Schweizer

Universität des Saarlandes

12 PUBLICATIONS 115 CITATIONS

SEE PROFILE



S. Shylesh

University of California, Berkeley

62 PUBLICATIONS 1,631 CITATIONS

SEE PROFILE



Werner R Thiel

Technische Universität Kaiserslautern

221 PUBLICATIONS 3,695 CITATIONS

SEE PROFILE

Nanoparticle Supported, Magnetically Recoverable Oxodiperoxo Molybdenum Complexes: Efficient Catalysts for Selective Epoxidation Reactions


Sankaranarayananpillai Shylesh,^a Julia Schweizer,^b Serhiy Demeshko,^c Volker Schünemann,^b Stefan Ernst,^a and Werner R. Thiel^{a,*}

^a Fachbereich Chemie, TU Kaiserslautern, Erwin-Schrödinger-Str., Geb. 54, 67663 Kaiserslautern, Germany
Fax: (+49)-631-205-4676; e-mail: thiel@chemie.uni-kl.de

^b Fachbereich Physik, TU Kaiserslautern, Erwin-Schrödinger-Str., Geb. 56, 67663 Kaiserslautern, Germany

^c Institut für Anorganische Chemie, Georg-August-Universität Göttingen, Tammannstraße 4, 37077 Göttingen, Germany

Received: April 8, 2009; Revised: June 17, 2009; Published online: August 5, 2009

 Supporting information for this article is available on the WWW under <http://dx.doi.org/10.1002/adsc.200900416>.

Abstract: Organic-inorganic hybrid heterogeneous nanocatalyst systems were synthesized by covalent anchoring of oxodiperoxo molybdenum complexes $[(L-L)MoO(O_2)_2]$ on silica coated magnetic nanoparticles as an active, magnetically separable epoxidation catalyst.

Keywords: epoxidation; heterogeneous catalysis; magnetic nanoparticles; molybdenum; surface functionalization

The selective transformation of alkenes into epoxides generates valuable starting materials for further functionalization and opens up an access to industrially important products such as polyethers, epoxy resins and surfactants.^[1] During the last decades, a series of homogeneous catalysts were identified to be active in this reaction. Among them molybdenum- and tungsten-based systems play an important role.^[2] In most cases, the regeneration of a homogeneous catalyst from a reaction mixture is difficult, causes costs and creates additional waste. Therefore it is worthwhile to investigate innovative approaches for catalyst heterogenization. This requires a detailed insight into the mechanism of the catalyzed reaction, to be sure that, for example, ligand dissociation will not lead to catalyst leaching.

Covalent grafting of a homogeneous catalyst on an insoluble porous solid support with high surface area is one method of choice in this context. It allows catalyst recovery by simple filtration.^[3] However, due to the diffusion of substrates and products through the pores of the support materials, a substantial decrease

in reaction rate is frequently observed compared to the homogeneous system.^[4] Such catalysts may also encounter further problems of solid phase-supported organic reactions: a reduced selectivity, a non-linear kinetic behaviour, a lack of complete recovery of the catalyst and difficulties in transferring standard solution phase conditions to the solid phase system.^[5]

One way to overcome this drawback is to keep the size of the support particles as small as possible. Therefore nanoparticles have recently emerged as efficient alternatives for the immobilization of homogeneous catalysts. Due to the high external surface areas of non-porous nanoparticles a high loading of catalytically active sites is guaranteed and diffusion will no longer limit the kinetics. Hence nanocatalysis may effectively bridge homogeneous and heterogeneous catalysis.^[6] Furthermore, nanometer-sized particles are often easily dispersible in solution by forming stable suspensions.^[7] However such suspensions of particles with less than 100 nm diameter are difficult to filter. Therefore expensive ultra-centrifugation is often the only way to separate product and catalyst.

Fabrication of core-shell magnetic nanoparticles has recently been subject of extensive research, since such materials combine the unique magnetic properties of the core together with the possibility to further functionalize the surface. This has motivated research to develop designed applications in different fields like bioseparation, drug delivery, MRI, catalysis and others.^[8] The specific advantages of magnetic nanomaterials are the following: a) a high specific surface, b) the active sites are mainly distributed on the “outer” surface of the support which avoids pore diffusion, c) the application of an external magnetic field enables the removal of the particles in a simple way.

In 2007 Hyeon and co-workers reported the first magnetically separable epoxidation catalyst based on Fe_2O_3 particles of about 400 nm diameter which were covered with a 50 nm layer of mesoporous silica, wherein molybdenum was impregnated.^[9] In the present paper we report novel, highly active and selective, magnetically recoverable catalysts based on covalently grafted molybdenum complexes.

For this purpose we used magnetic nanoparticles (MNP) of approximately 10 nm diameter which were prepared by the co-precipitation method.^[10] The particles were subsequently coated with a dense silica layer of 50 nm thickness, using tetraethoxysilane (TEOS) as the silica source and aqueous NH_3 as the hydrolysing agent. The silica layered system **SMNP** then offers the binding sites (Si–OH units) for the heterogenization of the molecular catalysts. For the grafting on the surface we used {(3-triethoxysilylpropyl)[3-(2-pyridyl)-1-pyrazolyl]acetamide} (TPPA)^[4c] and commercially available *N*-(2-aminoethyl)-3-aminopropyltriethoxysilane (AAPS) as chelating ligands. They were reacted with $\text{MoO}(\text{O}_2)_2 \cdot (\text{DMF})_2$ in dry CHCl_3 to yield the corresponding oxodiperoxomolybdenum complexes **1Mo** and **2Mo**, which were used for grafting on the silica surface of the nanoparticles and provided the functionalized systems **1Mo@SMNP** and **2Mo@SMNP** (Scheme 1).

The intermediates and the final molybdenum catalysts were characterized systematically by HR-TEM, field emission-scanning electron microscopy (FE-SEM), X-ray diffraction (XRD), FT-IR spectroscopy, Mössbauer and SQUID measurements.

High resolution-transmission electron microscopy (HR-TEM) images and electron diffraction patterns of the MNPs depict relatively uniform $\gamma\text{-Fe}_2\text{O}_3$ particles with an average size of ~10 nm (see Supporting Information). TEM images of the silica coated MNPs (SMNP) shows the typical core-shell structure with a uniform silica coating and a mean thickness of approximately 50 nm. The dense silica shell prevents the leaching of iron from the core during the epoxidation

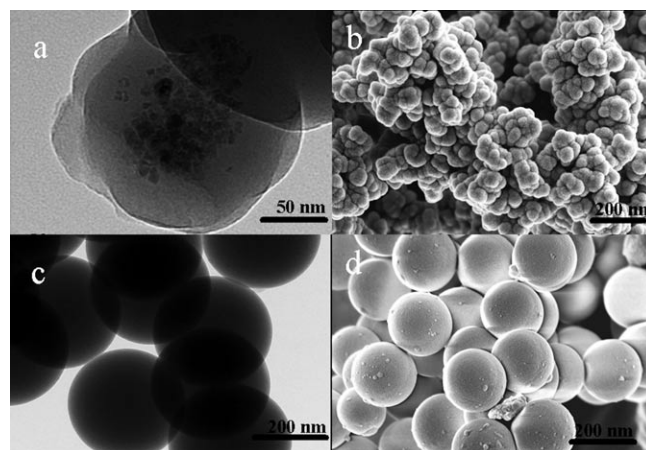


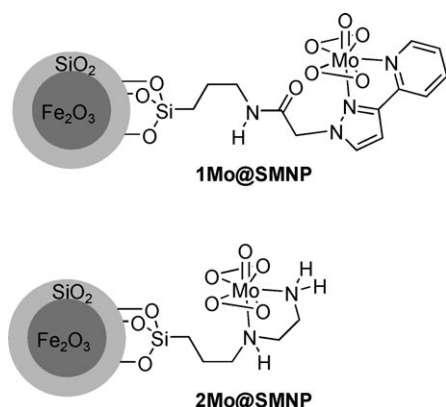
Figure 1. HR-TEM and FE-SEM images of SMNP particles (a, b) and silica nanospheres (c, d).

reactions and also assists in a stable anchoring of the silylating agents. Since the iron oxide nanoparticles tend to aggregate prior to or during the silica coating step, more than one magnetic core is trapped in the final particles (Figure 1 a). Such an architecture is advantageous in concentrating the core-shell particles with an external magnetic field after catalytic reactions.^[11] As expected the core-shell structure of the nanoparticles stays intact during the grafting reactions.

FE-SEM images reveals that the MNPs exhibits aggregated particles having rough external surfaces while after silica coating the particles exhibit smooth, spongy surfaces (Figure 1 b) showing the successful coating of silica over the magnetic nanoparticles. Energy dispersive X-ray (EDX) analysis of SMNP particles proves the presence of silica and iron, while after the grafting reaction, Fe, Si, N and Mo are present on the samples **1Mo@SMNP** and **2Mo@SMNP** which confirms the successful anchoring of the active sites (see Supporting Information). For comparison, silica nanospheres (SNS) of ~200 nm were also synthesized using a modified Stober method, without the iron core. The TEM and SEM images are also depicted in Figure 1.

XRD measurements of MNP exhibit diffraction peaks corresponding to the typical maghemite ($\gamma\text{-Fe}_2\text{O}_3$) structure while the silica layered systems **SMNP**, **1Mo@SMNP** and **2Mo@SMNP** show an additional broad band ($2\theta = 20\text{--}30$) for the amorphous silica (see Supporting Information).^[7] The average crystallite size of the $\gamma\text{-Fe}_2\text{O}_3$ particles was calculated to be ~9.3 nm by Scherrer's equation for the (311) reflection, which is in well accordance with the HR-TEM results.

Superparamagnetic particles are beneficial for magnetic separation, since they are strongly attracted by a magnetic field and retain no residual magnetism once



Scheme 1. Constitution of the SMNP derived catalysts.

the field is removed. The magnetism of **MNP**, **SMNP** and **1Mo@SMNP** particles was investigated by SQUID magnetometry. The field dependent magnetization curve at 300 K of the magnetic nanoparticles, exhibits no hysteresis revealing that the materials exhibit superparamagnetic behaviour at room temperature. As expected, the bare $\gamma\text{-Fe}_2\text{O}_3$ magnetic particles showed the highest magnetic value (saturation magnetization, M_s) of 56 emu g^{-1} (Figure 2). The M_s values of **SMNP** as well as **1Mo@SMNP** sample are decreased due to the silica coating and the layer of the grafted catalyst (18 emu g^{-1} and 15 emu g^{-1} for **SMNP** and **1Mo@SMNP**, respectively).^[12] The zero-field cooled (ZFC) and field-cooled (FC) magnetization under an applied field of 100 Oe between 2 and 300 K gave further confirmation about the superparamagnetism of the nanoparticles (see Supporting Information). The blocking temperature (T_B) was determined to be 215 K for **1Mo@SMNP** which according to related references was comparable to $\gamma\text{-Fe}_2\text{O}_3$ nanoparticles synthesized with a mean diameter of 10 nm.^[13]

Figure 3a shows the Mössbauer spectrum of **SMNP** recorded at 300 K. The spectrum was analyzed by a superposition of two components: (i) a doublet with an isomer shift $\delta = 0.36 \text{ mm s}^{-1}$ and a quadrupole splitting $\Delta E_Q = 0.50 \text{ mm s}^{-1}$ (component 1) and (ii) a broad magnetic sextet with parameters given in the Supporting Information (component 2). Component 1 in Figure 3 represents superparamagnetic single domain particles, the magnetic moments of which fluctuate with a relaxation time shorter than the time window of Mössbauer spectroscopy (*ca.* 10^{-7} s).^[14] Component 2 represents particles with magnetic moments which fluctuate with a relaxation time in the order of 10^{-7} s . Cooling down the sample to $T = 77 \text{ K}$ leads to a magnetic six line pattern with 80% contribution to the total spectral area. The parameters are given in Table S1 (Supporting Information).

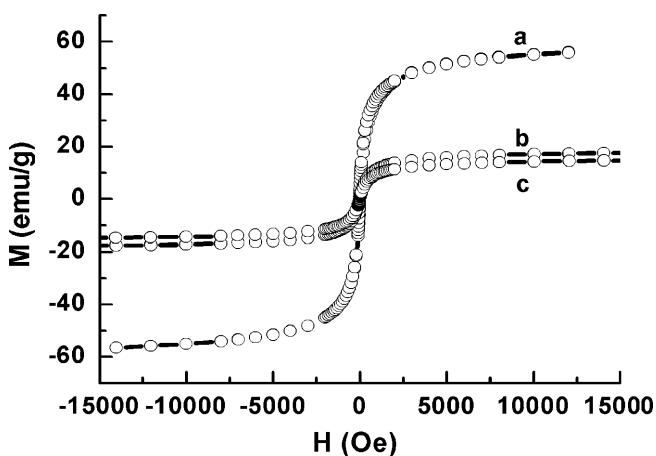


Figure 2. Field-dependent magnetization plots of (a) **MNP**, (b) **SMNP** and (c) **1Mo@SMNP**.

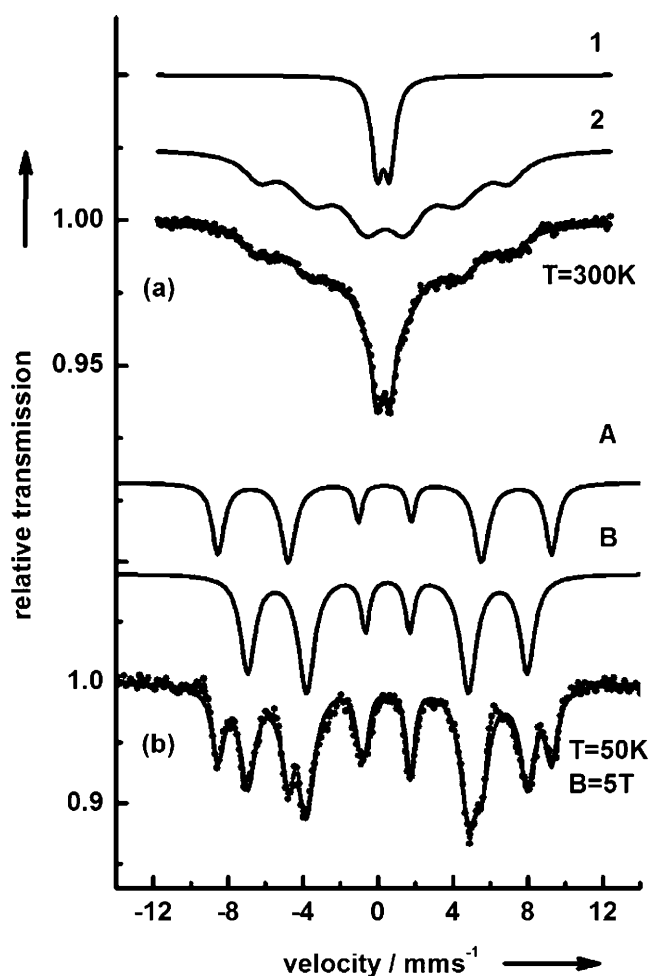


Figure 3. Mössbauer spectra of **SMNP** obtained at 300 K in zero magnetic field (a) and at 50 K in a field of 5 T applied perpendicular to the γ -beam (b). The solid lines are simulations with the parameters shown in the Supporting Information, Tables S1 and S2 assuming Lorentzian line shape.

To determine the iron oxide phase of the silica coated particles field-dependent Mössbauer spectra up to 5 T have been taken (see: Supporting Information). The Mössbauer spectrum obtained at 5 T (Figure 3b) shows two resolved magnetic sextets (component A and B) with $\delta_A = 0.36 \text{ mm s}^{-1}$ and $\delta_B = 0.50 \text{ mm s}^{-1}$ and hyperfine fields of $B_{hfA} \sim 55 \text{ T}$ and $B_{hfB} \sim 46 \text{ T}$. Component A represents high-spin Fe(III) ions located in the A-site of $\gamma\text{-Fe}_2\text{O}_3$ and component B represents high-spin Fe(III) ions in the B-site of the $\gamma\text{-Fe}_2\text{O}_3$ lattice.^[14a]

Obviously the external field of 5 T decreases the magnetic hyperfine field of the ions in the B-sites to a value of $\sim 46 \text{ T}$ which shows that the sign of B_{hfB} is negative. In turn the external field leads to an increase of the hyperfine field of the ions in the A-sites to $\sim 55 \text{ T}$, which shows that the sign of B_{hfA} is positive. Because B_{hf} is dominated by a negative Fermi contact contribution, an external field B leads to a decrease

in B_{hf} in the case of field parallel alignment of the magnetic moments. Thus Figure 3b shows that the magnetic moments of the Fe(III) B-sites of the ferrimagnetic particles are oriented almost parallel and those of the Fe(III) A-sites are oriented antiparallel to the external field of 5 T at $T=50$ K. Ferrimagnetic $\gamma\text{-Fe}_2\text{O}_3$ has a spinel (AB_2O_4) structure, but there are too few Fe(III) cations to fill all the A and B sites. Assuming that all vacancies are located on the B lattice gives a ratio of $A/B=0.60$, which is in exact agreement with the ratio of the relative spectral areas of components A and B in the spectrum displayed in Figure 3b (see also Table S2, Supporting Information).^[14a] Thus Mössbauer spectroscopy identifies the superparamagnetic particles as $\gamma\text{-Fe}_2\text{O}_3$ (maghemite). The presence of significant amounts of Fe_3O_4 ($\geq 5\%$) can be excluded since there is no evidence for spectral components representing Fe(II) ions.

The presence of the magnetic iron oxide inside **1Mo@SMNP** and **2Mo@SMNP** prevents analysis by solid state NMR spectroscopy. Therefore these hybrid materials were further characterized by IR spectroscopy and elemental analysis (see Supporting Information). The IR spectrum of **MNP** shows the Fe–O stretching absorption at 576 cm^{-1} . After coating with silica a new sharp band for the Si–O vibration appears at 1080 cm^{-1} . In the IR spectra of **1Mo@SMNP** and **2Mo@SMNP** absorptions at 3300 cm^{-1} (N–H), 2930 cm^{-1} (CH_2), 1640 cm^{-1} (C=O) and 1385 cm^{-1} were observed indicating the presence of the silylating groups.^[15] By determination of the nitrogen content, a catalyst loading of approximately 0.25 mmol g^{-1} (**1Mo@SMNP**) and 0.28 mmol g^{-1} (**2Mo@SMNP**) was calculated.

The activity of the organic/inorganic hybrid catalysts **1Mo@SMNP** and **2Mo@SMNP** was evaluated for the epoxidation of *cis*-cyclooctene. A series of different solvents like chloroform, toluene, acetonitrile, dioxane and different oxidizing agents like *tert*-butyl hydroperoxide (*t*-BuOOH) and hydrogen peroxide (H_2O_2) were investigated to evaluate the appropriate conditions with 1 mol% of the nanostructured system **1Mo@SMNP**. The combination of CHCl_3 and *t*-BuOOH gave the best conversions (see Supporting Information). These findings are consistent with the results obtained under homogeneous systems which we reported previously.^[16]

The AAPS-derived molybdenum catalyst **2Mo@SMNP** showed considerably lower conversion than the pyrazolopyridine-based **1Mo@SMNP** system (Table 1). There are two effects to be discussed in this context. As we could show previously a free coordination site at the molybdenum centre is required for the activation of the peroxide.^[17] Therefore bidentate ligands with one weaker donor centre will preferentially decoordinate and go into a monodentate coordination mode as we could show on a series of oxodiperoxo(pyrazolylpyridine)molybdenum complexes func-

Table 1. Epoxidation of olefins with *t*-BuOOH catalyzed by nano-molybdenum catalysts.^[a]

Entry	Alkene	Yield of epoxide [%] ^[b]	
		1Mo@SMNP	2Mo@SMNP
1	cyclooctene	96	58
2	cycloheptene	90	52
3	cyclohexene	82	57
4	styrene	72	46
5	1-octene	77	52

^[a] Reaction conditions: 1 mmol of alkene, 1.2 mmol of *t*-BuOOH, 1 mol% of catalyst, 5 mL of CHCl_3 , 6 h, reflux.

^[b] Yields were determined by GC-MS with respect to an internal standard (decane).

tionalized at the pyrazole ring. In **2Mo@SMNP** two electron-rich alkylamines are used to bind the molybdenum centre. On the other hand, it is known that alkylamines can catalytically be oxidized by molybdenum derived catalysts giving poor donor motifs such as nitrones, nitro or nitroso units.^[18]

To evaluate this enhancement, equivalent amounts of pyrazolyl pyridine oxodiperoxo molybdenum complexes were heterogenized on the silica nanospheres (**1Mo@SNS**), synthesized by the Stober method (Figure 1), as well as on MCM-41 (**1Mo@MCM-41**). In both cases, the conversion was found to be less than for **1Mo@SMNP**. The inherent difficulties in the total recovery of the catalyst limits their applications in consecutive cycles (see Supporting Information). An additional increase in activity may possibly arise from the presence of Lewis-acidic sites (here: Fe^{3+}) on the support.^[4c] The carbonyl group of the amide fragment of **1Mo@SMNP** or one of the peroxo ligands may interact with such sites. The improved catalytic activity of **1Mo@SMNP** compared to MCM-41 arises from the ideal exposition of the active sites on the surface of the nanoparticles which is almost similar to a quasi-homogeneous catalyst system. In contrast, the diffusion limitation or pore constraints in MCM-41 will devoid active sites for the substrate molecules.

Encouraged by the preliminary results obtained for cyclooctene, the epoxidation of further olefins was carried out under optimized conditions. As shown in Table 1, the molybdenum catalysts convert the olefins to the corresponding epoxides with good to excellent yield similar to the result for cyclooctene. As already observed for similar homogeneous oxodiperoxo molybdenum catalysts, the heterogenized systems convert especially olefins without any functional groups attached.^[19] This is due to the mechanism of the oxygen transfer.^[17,20]

For practical applications of heterogeneous catalyst systems, the stability and reusability are important factors. The **1Mo@SMNP** catalyst can be reused six



Figure 4. Magneto filtration of finely dispersed superparamagnetic **1Mo@SMNP** nanoparticles (*left*: shortly after the application of the magnet; *right*: 2 min later)

Table 2. Results of catalyst reuse experiments in the epoxidation of cyclooctene.

Run	1	2	3	4	5	6
1Mo@SMNP	96	96	95	93	93	92
2Mo@SMNP	58	58	54	51	50	47

times, by simple magnetic separation (Figure 4), without any deterioration of conversion and selectivity in the epoxidation reaction of cyclooctene, while the **2Mo@SMNP** catalyst shows a slightly decreasing trend in catalytic activity during reuse (Table 2). The bidentate 2-(1-alkyl-3-pyrazolyl)pyridine ligand exhibits a stronger affinity to the oxodiperoxo molybdenum complexes than the conventional AAPS ligand and thus enhances the conversion and stability of the molybdenum catalysts. The supernatant was not active for the epoxidation reactions at all which further indicates the truly heterogeneous nature of the **1Mo@SMNP** catalyst (see Supporting Information). However, it turned out to be difficult to reuse the non-magnetic hybrid catalysts **1Mo@SNS** and **1Mo@MCM-41** more than three times and their conversion decreased gradually during the reuse. The high catalytic activity and stability of the molybdenum catalyst relates in our opinion mainly to the better site isolation of the active catalytic sites, the relatively strong interaction between the chelating ligand and the molybdenum centre and to the covalent grafting between the organic ligand and the $\text{Fe}_2\text{O}_3/\text{SiO}_2$ support.

In summary, we have demonstrated that magnetic nanoparticle supported molybdenum species are efficient, easily recoverable catalysts for selective olefin epoxidation. The synthesis procedures are facile and are exemplified by the high catalytic activity and stability of the bidentate 2-(1-alkyl-3-pyrazolyl)pyridine ligand supported on SMNP. MCM-41 and silica nanoparticle supported Mo catalysts of similar loading and with a more simple diamine ligand like AAPS have turned out to give poorer results. We here have shown a strategy for recovery by magnetic separation

and the reuse which can be readily applied for the heterogenization of other homogenous ligands/catalysts.

Experimental Section

General Remarks

Unless otherwise stated, all manipulations were carried out under an inert atmosphere of nitrogen and the solvents were dried by standard methods. Reagents were purchased from Aldrich chemicals and were used without further purification.

Synthesis of Magnetic Nanoparticles (MNPs)

Ferrous chloride (0.25 g) and ferric chloride (0.5 g) were added to 20 mL of nitrogen-purged 2-propanol under stirring giving a yellowish orange solution. After 15 min of stirring, the temperature was raised to 80 °C and about 10 mL of aqueous NH_3 were added slowly. The colour of the solution turned to dark brown and the stirring was then continued for another 2 h. The synthesized magnetic nanoparticles were protected using oleic acid and dispersed in ethanol.

Synthesis of Silica Coated Magnetic Nanoparticles (SMNPs)

2.0 g of ethanol dispersed MNPs were diluted with 4 mL of deionized water and 20 mL of 2-propanol. The mixture was sonicated for approximately 5 min. To this well dispersed MNP solution, 1 mL of NH_4OH followed by 1 g of tetraethoxysilane were slowly added. The solution was stirred at room temperature for 4 h. The resulting material was separated by centrifugation and then redispersed in deionized water.

Synthesis of Silica Nanospheres (SNS)

To a solution of absolute ethanol (20 g) and deionized water (5 g), 1 g of NH_4OH was added and the mixture was stirred at room temperature. Under continuous stirring, the solution temperature was raised to 50 °C and 1.8 g of tetraethoxysilane were rapidly added and the mixture was stirred for further 4 h. The solvent was removed under vacuum and the resulting white powder was dried at 100 °C.

Synthesis of (3-Triethoxysilylpropyl)[3-(2-pyridyl)-1-pyrazolyl]acetamide (TPPA)

The silylated ligand was synthesized according to ref.^[21] The spectroscopic data were in accordance with the published data.

Synthesis of Oxodiperoxo{(3-triethoxysilylpropyl)[3-(2-pyridyl)-1-pyrazolyl]acetamide}molybdenum (VI) (1Mo)

0.1 g of TPPA was stirred with 0.09 g (0.30 mmol) of $\text{MoO}(\text{O}_2)_2 \cdot (\text{DMF})_2$ dissolved in 50 mL of CHCl_3 at room temperature for 24 h. The yellow, solid material obtained

was then separated, washed repeatedly with CHCl_3 , CH_2Cl_2 and then dried under vacuum.

Grafting of 1Mo over SMNPs (1Mo@SMNP)

0.1 g of **1Mo** dissolved in 5 mL of dry CHCl_3 were added to a suspension of 0.6 g of SMNP in 30 mL of dry toluene. The mixture was then stirred at 90°C under nitrogen atmosphere for 12 h. The solid material obtained was magnetically separated, washed repeatedly with toluene and CHCl_3 to remove the unanchored species and then dried under vacuum.

Synthesis of Oxodiperoxo{(N-(2-aminoethyl)-3-aminopropyltriethoxysilane)molybdenum(VI) (2Mo)

0.1 g of APTS were stirred with 0.09 g (0.30 mmol) of $\text{MoO}(\text{O}_2)_2 \cdot (\text{DMF})_2$ dissolved in 50 mL of CHCl_3 at room temperature for 24 h. The yellow, solid material was separated, washed repeatedly with CHCl_3 and then dried under vacuum.

Grafting of 2Mo over SMNPs (2Mo@SMNP)

0.1 g of **2Mo** in 5 mL of dry CHCl_3 was added to a suspension of 0.6 g of SMNP in 30 mL of dry toluene. The mixture was then stirred at 90°C under a nitrogen atmosphere for 12 h. The solid material was then magnetically separated, washed repeatedly with toluene and CHCl_3 to remove the unanchored species and dried under vacuum.

Acknowledgements

The Alexander von Humboldt-Foundation is gratefully acknowledged for a research grant to S.S. This work was further supported by the joint research project "NanoKat" at the TU Kaiserslautern.

References

- [1] a) Q. H. Xia, H.-Q. Ge, C.-P. Ye, Z.-M. Liu, K.-X. Su, *Chem. Rev.* **2005**, *105*, 1603; b) R. A. Sheldon, *J. Mol. Catal.* **1980**, *7*, 107; c) A. Corma, *Chem. Rev.* **1997**, *97*, 2373; d) T. Mallat, A. Baiker, *Chem. Rev.* **2004**, *104*, 3037.
- [2] a) B. S. Lane, K. Burgess, *Chem. Rev.* **2003**, *103*, 2457; b) K. A. Jorgensen, *Chem. Rev.* **1989**, *89*, 431; c) G. Strukul, (Ed.), *Catalytic oxidation with hydrogen peroxides as oxidant*, Kluwer, Rotterdam, **1992**; d) F. E. Kühn, A. D. Lopes, A. M. Santos, E. Herdtweck, J. J. Haider, C. C. Romao, A. G. Santos, *J. Mol. Catal. A. Chem.* **2000**, *151*, 147; e) W. R. Thiel, T. Priermeier, *Angew. Chem.* **1995**, *107*, 1870; *Angew. Chem. Int. Ed. Engl.* **1995**, *34*, 1737.
- [3] a) A. Corma, H. Garcia, *Chem. Rev.* **2002**, *102*, 3837; b) D. E. DeVos, M. Dams, B. F. Sels, P. A. Jacobs, *Chem. Rev.* **2002**, *102*, 3615; c) L. Yin, J. Liebscher, *Chem. Rev.* **2007**, *107*, 133; d) A. Taguchi, F. Schüth, *Microporous Mesoporous Mater.* **2005**, *77*, 1.
- [4] a) P. Ferreira, I. S. Gonçalves, F. E. Kühn, A. D. Lopes, M. A. Martins, M. Pillinger, A. Pina, J. Rocha, C. C. Romao, A. M. Santos, T. M. Santos, A. A. Valente, *Eur. J. Inorg. Chem.* **2000**, 2263; b) C. D. Nunes, A. A. Valente, M. Pillinger, A. C. Fernandes, C. C. Romao, I. Rocha, I. S. Gonçalves, *J. Mater. Chem.* **2002**, *12*, 1735; c) M. Jia, A. Seifert, W. R. Thiel, *Chem. Mater.* **2003**, *15*, 2174; d) A. Sakthivel, J. Zhao, G. R. Sieber, M. Hanzlik, A. S. T. Chiang, F. E. Kühn, *Appl. Catal. A. Gen.* **2005**, *281*, 267.
- [5] Y. Zheng, P. D. Stevens, Y. Gao, *J. Org. Chem.* **2006**, *71*, 537.
- [6] a) G. A. Somorjai, A. M. Contreras, M. Montano, R. M. Rioux, *Proc. Natl. Acad. Sci. USA* **2006**, *103*, 10577; b) D. Astruc, F. Lu, J. R. Aranzas, *Angew. Chem.* **2005**, *117*, 8062; *Angew. Chem. Int. Ed.* **2005**, *44*, 7852.
- [7] a) F. Raimondi, G. G. Scherer, R. Kotz, A. Wokaun, *Angew. Chem.* **2005**, *117*, 2228; *Angew. Chem. Int. Ed.* **2005**, *44*, 2190; b) Y. Piao, Y. Jang, M. Shokouhimehr, I. S. Lee, T. Hyeon, *Small*, **2007**, *3*, 255; c) S. U. Son, I. K. Park, J. Park, T. Hyeon, *Chem. Commun.* **2004**, 778; d) Y. Li, E. Boone, M. A. El-Sayed, *Langmuir* **2002**, *18*, 4921; e) M. Moreno-Manas, R. Pleixats, *Acc. Chem. Res.* **2003**, *36*, 638.
- [8] a) A. H. Lu, E. L. Salabas, F. Schüth, *Angew. Chem.* **2007**, *119*, 1242; *Angew. Chem. Int. Ed.* **2007**, *46*, 1222; b) A. H. Lu, F. Schüth, *Adv. Mater.* **2006**, *18*, 1793; c) T. Hyeon, *Chem. Commun.* **2003**, 927; d) J. R. Weissleder, K. Kelly, E. Y. Sun, T. Schatland, I. Josephson, *Nat. Biotechnol.* **2005**, *23*, 1418; e) D. K. Yi, S. S. Lee, J. Y. Ying, *Chem. Mater.* **2006**, *18*, 2459; f) R. Abu-Reziq, H. Alper, D. Wang, M. L. Post, *J. Am. Chem. Soc.* **2006**, *128*, 5279; g) M. Kawamura, K. Sato, *Chem. Commun.* **2007**, 3404; h) C. Ó. Dálaiigh, S. A. Corr, Y. Gun'ko, S. J. Connon, *Angew. Chem.* **2007**, *119*, 4407; *Angew. Chem. Int. Ed.* **2007**, *46*, 4329; i) A. Hu, G. T. Yee, W. Lin, *J. Am. Chem. Soc.* **2005**, *127*, 12486; j) C. S. Gill, B. A. Price, C. W. Jones, *J. Catal.* **2007**, *251*, 145.
- [9] M. Shokouhimehr, Y. Piao, J. Kim, Y. Jang, T. Hyeon, *Angew. Chem.* **2007**, *119*, 7169; *Angew. Chem. Int. Ed.* **2007**, *46*, 7039.
- [10] a) Y. S. Kang, S. Risbud, J. F. Rabolt, P. Stroeve, *Chem. Mater.* **1996**, *8*, 2209.
- [11] Typical core-shell structures are generally observed on small scale experiments and were difficult to reproduce the architecture on large scale synthesis of magnetic silica nanocomposites.^[8]
- [12] D. K. Yi, S. S. Lee, G. C. Papaefthymiou, J. Y. Ying, *Chem. Mater.* **2006**, *18*, 614.
- [13] M. D. Mukadam, S. M. Yusuf, P. Sharma, S. K. Kulshreshtha, *J. Magn. Magn. Mater.* **2004**, *272*, 1401.
- [14] a) N. N. Greenwood, T. C. Gibb, *Mössbauer Spectroscopy*, Chapman and Hall, London, **1971**; b) S. Morup, J.-A. Dumesic, H. Topsoe, *Applications of Mössbauer Spectroscopy*, Vol. II, (Ed.: R. L. Cohen), Academic Press, New York, **1980**, pp 1–53; c) V. Schünemann, H. Paulsen, *Applications of Physical Methods to Inorganic and Bioinorganic Chemistry*, (Eds.: R. A. Scott, C. M. Lukehart), Wiley InterScience, New York, **2007**, pp 243–270.
- [15] a) M. C. Burleigh, M. A. Markowitz, M. S. Spector, B. P. Gaber, *J. Phys. Chem. B* **2001**, *105*, 9935; b) S.

- Huang, P. Yang, Z. Cheng, C. Li, Y. Fan, D. Kong, J. Lin, *J. Phys. Chem. C* **2008**, *112*, 7130.
- [16] a) W. R. Thiel, M. Angstl, T. Priermeier, *Chem. Ber.* **1994**, *127*, 2373; b) W. R. Thiel, J. Eppinger, *Chem. Eur. J.* **1997**, *3*, 696.
- [17] A. Hroch, G. Gemmecker, W. R. Thiel, *Eur. J. Inorg. Chem.* **2000**, *3*, 1107.
- [18] W. R. Thiel, *Coord. Chem. Rev.* **2003**, *245*, 95.
- [19] W. R. Thiel, M. Angstl, N. Hansen, *J. Mol. Catal. A: Chem.* **1995**, *103*, 5.
- [20] a) W. R. Thiel, T. Priermeier, *Angew. Chem.* **1995**, *107*, 1870; *Angew. Chem. Int. Edt. Engl.* **1995**, *34*, 1737; b) W. R. Thiel, M. Barz, H. Glas, A.-K. Pleier, *Olefin Epoxidation Catalyzed by Molybdenum Peroxo Complexes: A Mechanistic Study*, in: *Peroxide Chemistry: Mechanistic and Preparative Aspects of Oxygen Transfer*, (Ed.: W. Adam), Wiley-VCH, Weinheim, p 433, **2000**.
- [21] M. Jia, W. R. Thiel, *Chem. Commun.* **2002**, 2392.
-